

AD 625894

SEMIANNUAL TECHNICAL SUMMARY REPORT

30 NOVEMBER 1965

Dynamic Optical Properties of Laser Materials

by

J. W. Carson
L. G. Komai

Contract No. Nonr-4878(00)
ARPA Order No. 306
Project Code No. 4730

code 1

CLEARINGHOUSE	
FOR FEDERAL SCIENCE AND TECHNICAL INFORMATION	
Receipt	Number
\$ 1.00	0.50 25 BOM
ARCHIVE COPY	

Prepared for

Office of Naval Research
Department of the Navy
Washington 25, D. C.

This research is part of Project DEFENDER under joint sponsorship of the Advanced Research Projects Agency, the Office of Naval Research, and the Department of Defense.

Reproduction in whole or in part is permitted for any purpose of the United States Government

AEROSPACE GROUP

Hughes Aircraft Company



Culver City, California

SEMIANNUAL TECHNICAL SUMMARY REPORT

30 NOVEMBER 1965

Dynamic Optical Properties of Laser Materials

by

J. W. Carson
L. G. Komai

Contract No. Nonr-4878(00)
ARPA Order No. 306
Project Code No. 4730

Prepared for

Office of Naval Research
Department of the Navy
Washington 25, D. C.

ABSTRACT

The results of temperature profile investigations in DL quality Linde ruby using non-resonant interferometric techniques are described. This constitutes the first part of an overall study of dynamic optical distortions in laser materials. Other investigations will include gain profile studies as well as polariscopic measurements of strain-birefringence. Preliminary gain studies are presented.

CONTENTS

I.	INTRODUCTION	1
II.	RESEARCH PROGRAM	2
	A. General Approach.	2
	1. Interferometry	2
	2. Gain Measurements	6
	B. Experimental Considerations	7
	1. Excitation Cavity	7
	2. Twyman-Green Interferometry	9
	3. Gain Probe Apparatus	9
	C. Results	12
	1. Temperature Profiles	12
	2. Preliminary Gain Studies	16
	REFERENCES	17
	APPENDIX A	18

ILLUSTRATIONS

Figure 1.	Interferometer II	3
Figure 2.	Interferometer I	5
Figure 3.	Cross-section of cloverleaf cavity	8
Figure 4.	Cavity with sidewall removed	8
Figure 5.	Pump light waveform	8
Figure 6.	Twyman-Green interferometer	10
Figure 7.	Fringe rate measurement setup	11
Figure 8.	Gain measurement setup	11
Figure 9.	Temperature profiles in ruby as a function of pump energy	13
Figure 10.	Temperature profiles in ruby as a function of pump energy	13
Figure 11.	Fringe rates as a function of pump energy	15
Figure 12.	Typical fringe motion as displayed on scope for probe beam along ruby axis	15
Figure A-1.	Definition of interferometer coordinates	19

I. INTRODUCTION

This report covers the effort of the first half year on Contract Nonr 4878(00) entitled "Dynamic Optical Properties of Laser Materials". The objective of this program is to experimentally determine the degree of degradation in the optical quality of laser materials under high output energy operation. The endeavor also has as its goal the correlation of the observed effects of degradation with the dynamic processes which occur in the severe environment of the requisite level of optical pump excitation.

The experimentation to date has been carried out using ruby as the laser material and has sought to establish the thermal profile in the active medium due to optical pumping. Preliminary studies in the associated gain profiles were also performed in order to gauge the deposition of the pump radiation in the ruby rod.

Interferometric fringe rate measurements were used extensively in the investigation of the temperature distributions. The gain distributions across the rod diameter were determined using oscillator-amplifier methods. A discussion of the experimental techniques used, the apparatus, and the results obtained is presented.

II. RESEARCH PROGRAM

A. GENERAL APPROACH

1. Interferometry

When laser materials are subjected to the intense environment of high-level pump fluxes, marked degradations in optical quality occur which manifest themselves by the deformations in the radiation wavefronts passing through the activated medium. Gas laser interferometry has been found to be quite effective in following the time development of these variations. Many detection methods can be used to display the results of such experimentation. High speed framing techniques, streak camera techniques, and photometric techniques all have their individual merits, and there are trade-offs possible among them in sensitivity, in ease of accumulating data, and in the interpretation of the results. In our experimentation we chose the last method as being a convenient, fast, and inexpensive method for investigating the thermal distributions in laser rods caused by optical pumping. In this section we present the analysis upon which our studies were based.

Consider the interferometer shown schematically in Figure 1 (Interferometer II). The cylindrical laser sample is excited in a geometry that has axial symmetry so that uniform pumping along the rod axis results. The interference pattern formed at the screen S is observed through the small aperture A. The changes in optical path during pumping are related to the movement of the interference fringes across this aperture behind which is situated a photodetector. The movement is recorded with an oscilloscope camera as an amplitude modulation. The sole requirement for the technique to be effective is that the pinhole diameter be small compared to a fringe width.

It is shown in the Appendix that the fringe rate (called ν_{II}) which results from this interferometer can be written as:

$$\nu_{II} = \frac{2n\ell}{\lambda_0} \left\{ \left[\frac{(n-1)}{n} \alpha_\ell + \alpha_n \right] \frac{\partial T}{\partial t} + \frac{1}{n} \frac{\partial n}{\partial N_0} \frac{\partial N_0}{\partial t} \right\} + \frac{2}{\lambda_0} \frac{d}{dt} [L_2 - L_1]$$

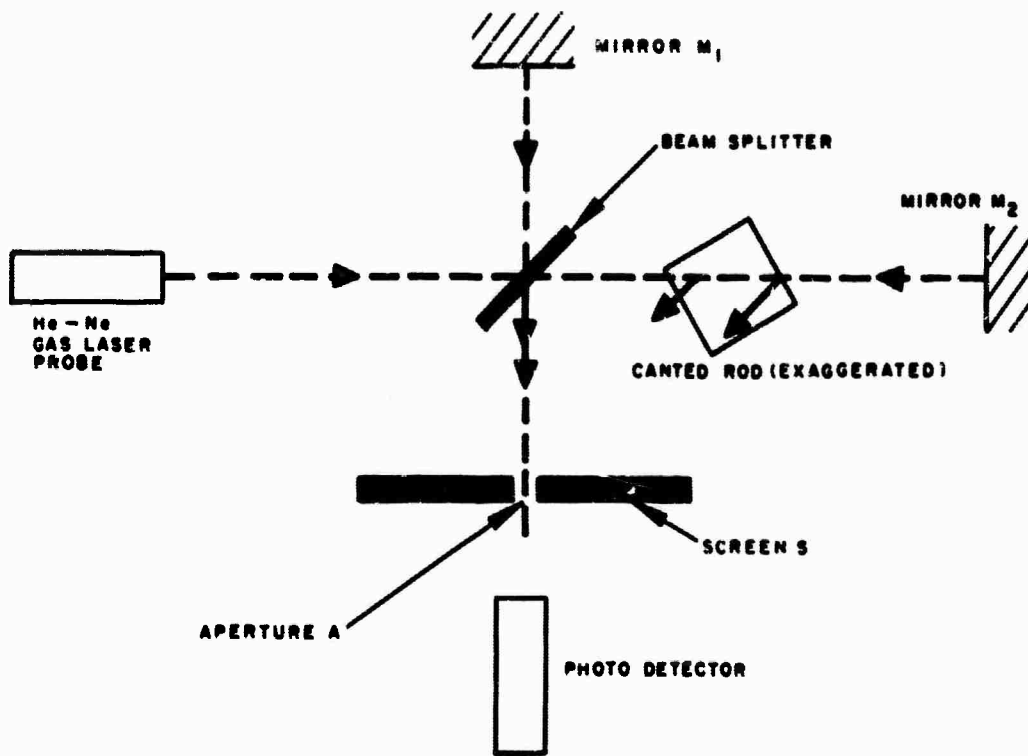


Figure 1. Interferometer II.

where

n = refractive index at λ_0 , the probe wavelength

l = initial rod length

L_1, L_2 = arm lengths of the interferometer

N_0 = ground-state population of the laser medium

T = temperature

$$\alpha_l \equiv \frac{1}{l} \frac{dl}{dT}$$

$$\alpha_n(\lambda) \equiv \frac{1}{n(\lambda)} \frac{dn(\lambda)}{dT}$$

The first term in ∂T describes the contribution to the fringe rate of the thermal expansion and refractive-index changes for a temperature rise ∂T in a time ∂t . With a constant-intensity pump, the temperature increases linearly with time for the pump duration, and the fringe rate should then be a constant for each pump power. The second term in dN_0/dt describes the effect on refractive index of a highly-depleted ground-state population. In general, this does not result in a uniform fringe rate since neither the depletion rate dN_0/dt nor $\partial n/\partial N_0$ may a priori be considered to be constant for the entire pump period. The constancy of ν_{II} may indicate which of these effects dominate. The last term in L_1 and L_2 accounts for the mechanical vibrations of the mirrors M_1 and M_2 resulting because of shocks transferred from the laser head. This has been observed to give rise to highly irregular fringe movements with periodicities of several hundred microseconds and rise times on the order of a millisecond. It is important that the pump period be made short compared with this rise time, and that the mirrors be shock-insulated from the laser head. The rise time is characteristic of the particular mechanical coupling that exists between the interferometric components. Next, consider a second interferometer, Figure 2, which leads to a fringe rate, ν_I , given by (see Appendix):

$$\nu_I = \frac{2nl}{\lambda_0} \left\{ (\alpha_l + \alpha_n) \frac{\partial T}{\partial t} + \frac{1}{n} \frac{\partial n}{\partial N_0} \frac{\partial N_0}{\partial t} \right\}$$

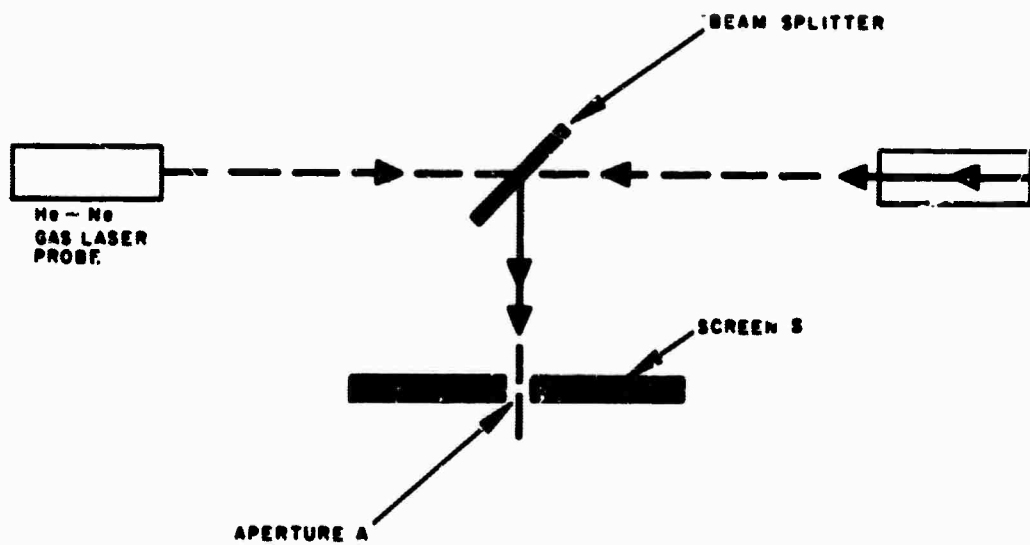


Figure 2. Interferometer I.

This simple interferometer produces good-visibility fringes resulting from interference between the beams reflected 180° with respect to the forward probe beam direction. (The visibility of the fringes in the forward direction is very poor.) Rod end reflectivities of about 5 percent are sufficient to establish fringe patterns. Since there are no external mirrors in this arrangement, the effects of the mechanical instabilities are minimized. The same arguments presented for ν_{II} on the constancy of the fringe rate also apply here.

If now we characterize the pump excitation to be a constant value P over a pump period Δt_p (a situation that was well approximated in practice), and ask for the temperature rise ΔT due to this excitation, we can write for ν_I and ν_{II}

$$\nu_{II} \cong \frac{2nl}{\lambda_o} \left[\frac{n-1}{n} \alpha_l + \alpha_n \right] \frac{\Delta T}{\Delta t_p}$$

$$\nu_I \cong \frac{2nl}{\lambda_o} \left[\alpha_l + \alpha_n \right] \frac{\Delta T}{\Delta t_p}$$

where the term due to mechanical instabilities has been dropped. Solving for ΔT , we have that:

$$\Delta T = \frac{\lambda_o}{2l\alpha_l} [\nu_I - \nu_{II}] \Delta t_p$$

With each transverse position of the probe beam relative to the sample axis, different fringe rates can be determined from which the associated temperature rise can be calculated. It is in this fashion that the thermal profiles were determined as a function of input energy.

2. Gain Measurements

A dynamic measurement of gain can be obtained by measuring the input and output intensities of a probe pulse at the amplifier wavelength. The gain profile measurements thus consist of the careful and systematic determination of the amplifier's gain (at a given pump energy) across a diameter or chord of the laser rod. By means of the beam splitters, calibrated phototubes, and matched scope amplifiers

the numerical gain can be directly evaluated. The sensitivity in measuring the inversion distribution is a function of the probe beam diameter which can be adjusted. The radial probing is accomplished by moving the aperture in an otherwise rigid and unchanged optical system to minimize and eliminate realignment or parallax errors.

B. EXPERIMENTAL CONSIDERATIONS

1. Excitation Cavity

Previous work in this laboratory indicated that a cavity of the cloverleaf type leads to reasonably uniform pump light distributions. On this basis a four-element cloverleaf cavity was built. A cross-section of the cavity is shown in Figure 3, and a picture of the fabricated unit in Figure 4. By modification of the sample holders, the unit can accommodate laser rods with diameters up to 5/8 inch and lengths up to 5 inches. The laser rod is held in the holders with white silicone rubber "O" rings. The holders are sealed to the cavity end-walls with "O" rings, as is also the protective Pyrex tube. The flashtubes are cooled by forced air while the laser rod can be either air-cooled or liquid-immersed. The flashtubes used so far have been EG&G FX 47-B linear tubes.

The energy source for the cavity is a 75 kJ power supply built by this laboratory (Contract Nonr 3920(00)). It has an output impedance of 1.5Ω with a pulse width of 1.1 ms. With the four flashtubes connected in series, there is an effective impedance match between power supply and flashtubes. The light output waveshape is shown in Figure 5. The light intensity is constant over most of the pump pulse. The power supply in the charged state does not recharge to correct for capacitor leakage losses. This limits the precision of repeating a given input pump energy to the error associated with reading the power supply voltmeter (about $\pm 1/2$ percent).

Preliminary work in the first quarter with 5/8 inch diameter by 5 inches length ruby showed the importance of optical quality. The fringe patterns in the Twyman-Green interferometer were severely distorted; in addition, the fringe contrast was rather poor because of

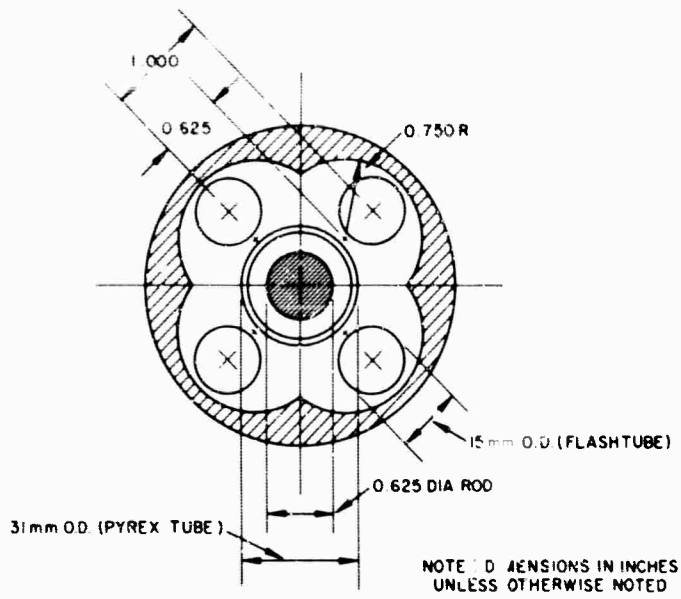


Figure 3. Cross-section of cloverleaf cavity.

Figure 4. Cavity with sidewall removed.

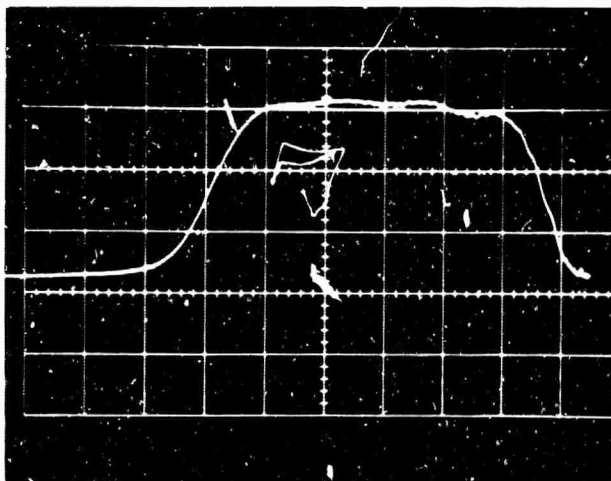
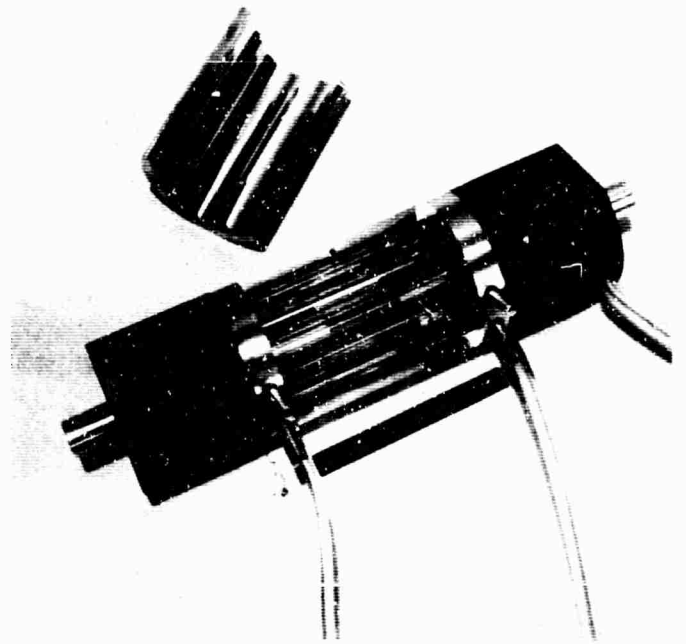


Figure 5. Pump light waveform (horizontal scale is 200 microseconds per cm).

absorption and scattering at $6328 \overset{\circ}{\text{Å}}$. To minimize these effects, it was decided to work with 5/8 inch by 2 inch length ruby of the best optical quality available. The results to be reported on are for 90° DL quality ruby from the Linde Division of Union Carbide Corporation.

2. Twyman-Green Interferometry

The temperature profile measurements were made using a Twyman-Green interferometer containing the excitation cavity in one arm (following the technique described in the previous section). The interferometer is shown in Figure 6. The two 100 percent reflecting mirrors and 50/50 beam splitter were mounted in gimbals secured to a 1 inch thick aluminum plate. This plate was shock-mounted to a base plate on which the cavity was mounted. This minimized the coupling of flashlamp-induced shocks to the interferometer mirrors during the pump period. The cavity was in a mount having several degrees of freedom in both translation and rotation.

A diagram of the complete setup is shown in Figure 7. The interferometer light source was a Spectra Physics gas laser Model 130. The wideband filter in front of the gas laser was found to be necessary to prevent oscillation at $6943 \overset{\circ}{\text{Å}}$ off the gas laser optics. The cavity was oriented almost normal to the probe beam such that the reflections from the front and back faces of the ruby did not overlap the interferometer fringe pattern. In this manner it was possible to measure ν_{I} and ν_{II} simultaneously.

3. Gain Probe Apparatus

Figure 8 shows a diagram of the equipment for this measurement. For accurate timing control of the pulse probe, a Q-switch is useful. Initially, a passively Q-switched cell containing cryptocyanine in propanol was used. As will be discussed later, this does not appear to be without its own undesirable characteristics. Hence, a Kerr cell or rotating mirror may be more satisfactory. A normal laser probe containing a number of closely spaced pulses also can be used, and the input and output signals integrated.

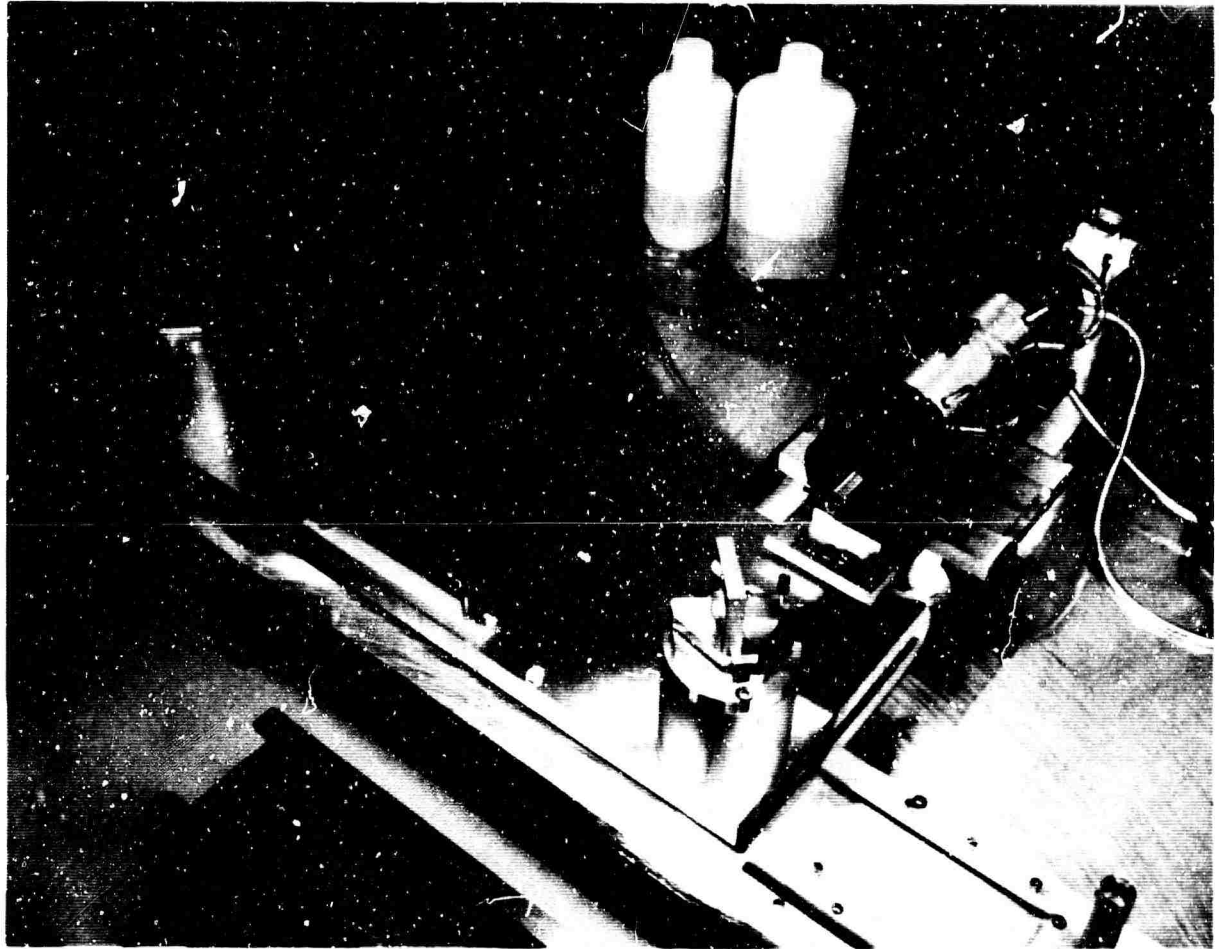


Figure 6. Twyman-Green interferometer.

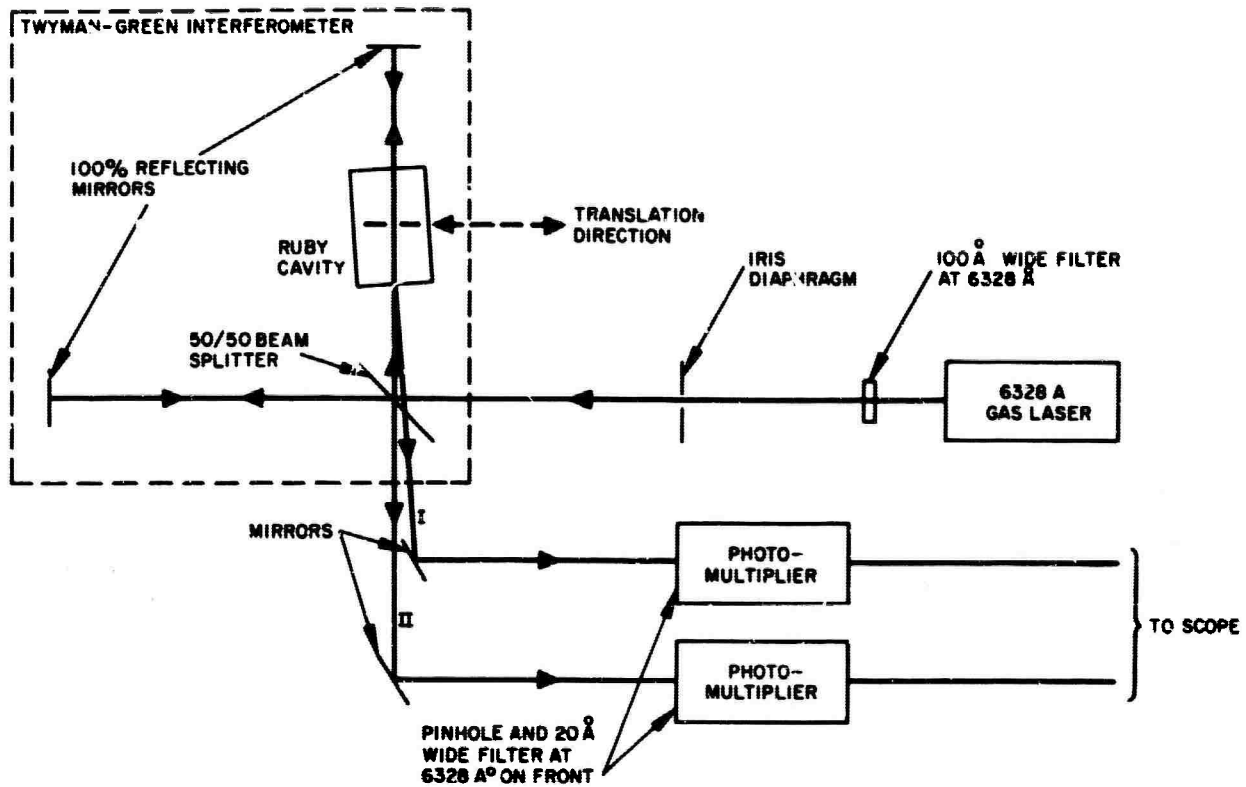


Figure 7. Fringe rate measurement setup.

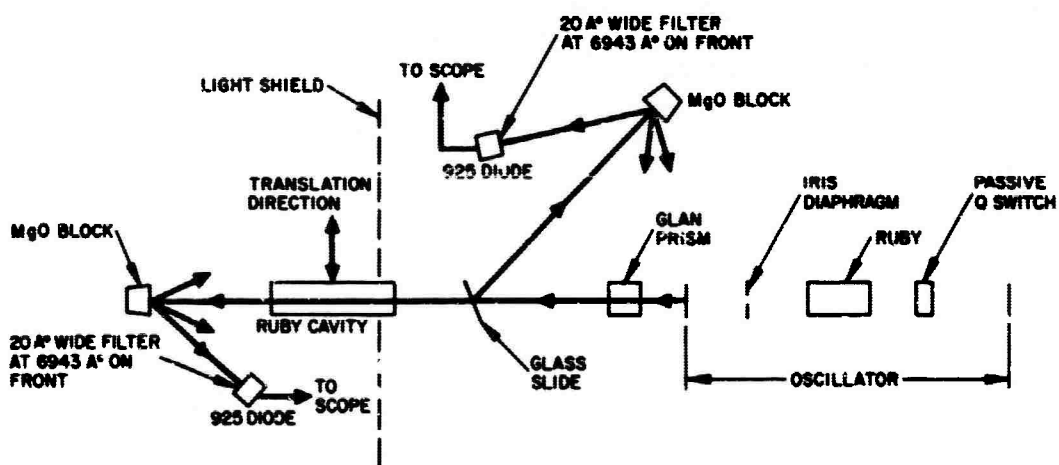


Figure 8. Gain measurement setup.

C. RESULTS

1. Temperature Profiles

The change in temperature for a given axial position of the ruby rod may be determined from ν_I or ν_{II} alone, or $\nu_I - \nu_{II}$. Experimentally it was found that turbulence during the pump period in the air paths just outside the ruby influenced ν_{II} . To minimize this, aluminum tubes were inserted in each end of the cavity to prevent cooling air and/or flashlamp-caused air turbulence from entering these areas. Since a small effect might still exist, ΔT was calculated from ν_I , for this depends only on what occurs in the ruby itself.

The cavity was moved normal to the probe beam (beam about 1/16 inch in diameter) to scan along a diameter. For the results reported here, the ruby had no resonant flux through it. The pump pulse had a total length of 1.1 milliseconds and was flat over about 800 microseconds. All fringe rate measurements were made in an interval of several hundred microseconds centered about a point 700 microseconds from the beginning of the pump pulse. The polarization of the gas laser probe was normal to the principal section of the ruby.

Typical temperature profile results are shown in Figure 9. There is a small increase in temperature from center to edge which depends somewhat on the pump energy level. A 5 percent increase is typical. Figure 9 is for the probe beam in a plane through the ruby center and two oppositely oriented flashtubes. These measurements were also taken for a plane through the ruby center and midway between two adjacent flashlamps. The results, shown in Figure 10, were the same as in Figure 9 within experimental error. A given fringe rate measurement was repeatable to ± 2 to 3 percent. All data were taken with the ruby immersed in water. A gravity flow system was used during the pump period so that the water was in continual motion. This, plus the addition of a small amount of Eastman Photoflo solution to the water, prevented the accumulation of air bubbles in the immersion cell.

The calculation of ΔT from the measured fringe rates assumes the dominance of the thermal variation in ruby length and index of

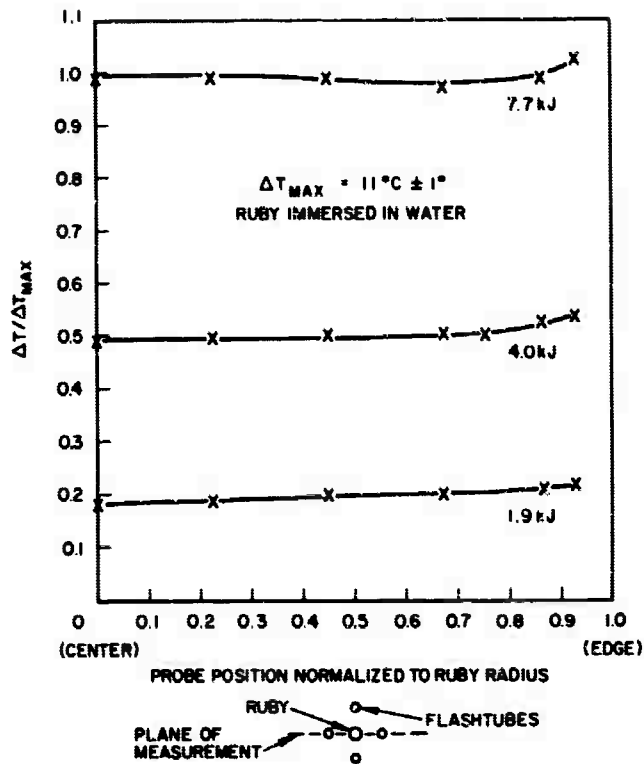


Figure 9. Temperature profiles in ruby as a function of pump energy.

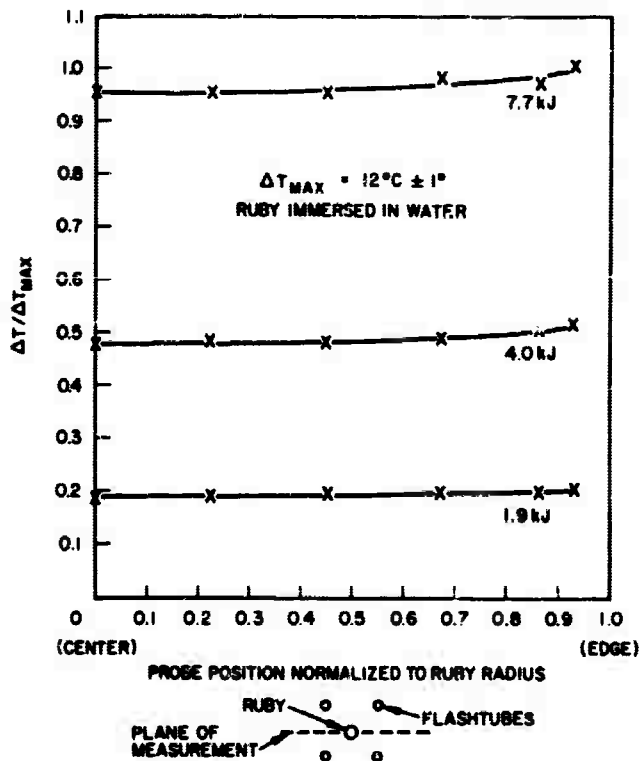


Figure 10. Temperature profiles in ruby as a function of pump energy.

refraction over temperature gradient effects. On this basis ν_I and ν_{II} would be expected to be linear with input pump energy. Figure 11 shows that ν_I and ν_{II} are indeed linear with pump energy over the range measured so far. The ratio ν_I/ν_{II} can be expressed in terms of α_n , α_l , and n . Using reported values for these,¹ the calculated value for the ratio is found to be 1.3. The measured value agrees with this. These results suggest that for the pumping levels used so far the change in optical quality is mainly caused by the thermal change in ruby length and refractive index. The results also suggest that thermal gradient effects are small. This agrees with previous work done in this laboratory² and elsewhere.¹

The temperature profile results show that the cloverleaf cavity configuration chosen does produce a high degree of uniformity of pump flux throughout the ruby. Improvements on it would be small and not too easy to achieve. Given this sort of situation, it is then of interest to inquire about the distortion in the phase front across the ruby in excess of that caused by the above described effects. It is possible to get an idea of the magnitude of this distortion (presumably related to strain-induced birefringence) by further inspection of the fringe motion photographs. From the definition of ν_I , it can be seen that the total single pass phase shift $\Delta\phi$ (where $\phi = 2\pi n l / \lambda_0$) is given by

$$\Delta\phi = \frac{[2\pi\nu_I\Delta t]}{2} = \pi\nu_I\Delta t$$

where the two in the denominator appears because $\Delta\phi$ is measured twice in Interferometer I. This shows that, if the previous assumptions about thermal change in length, etc., are correct, the total change in phase should be just proportional to ν_I . The total phase change from the beginning of the pump to any later point, timewise, can be determined by counting the number of fringes in the scope photographs (see Figure 12 for a typical scope photograph. It is found, going from the ruby center out, that the total phase change (by counting the number of fringes) increases by roughly the same ratio as the fringe rate. The difference in the two is within the reading error of the fringe rates.

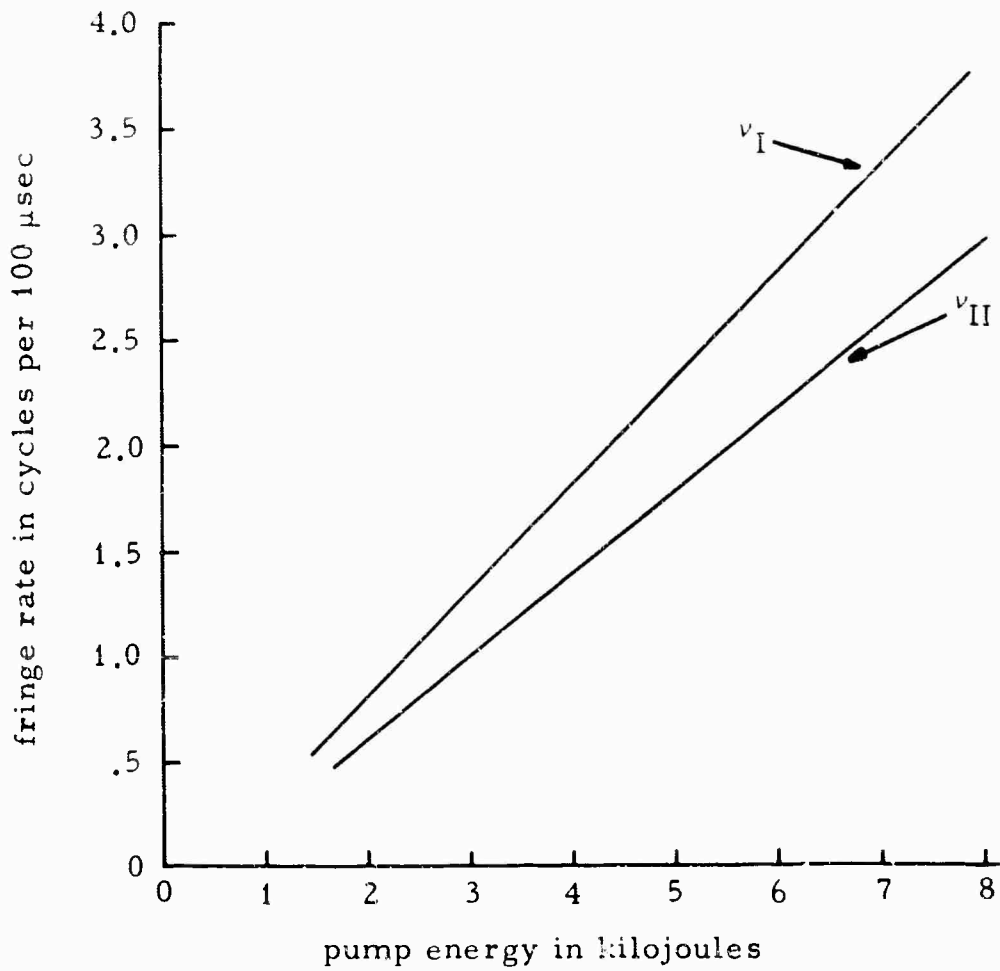


Figure 11. Fringe rates as a function of pump energy (along ruby axis).

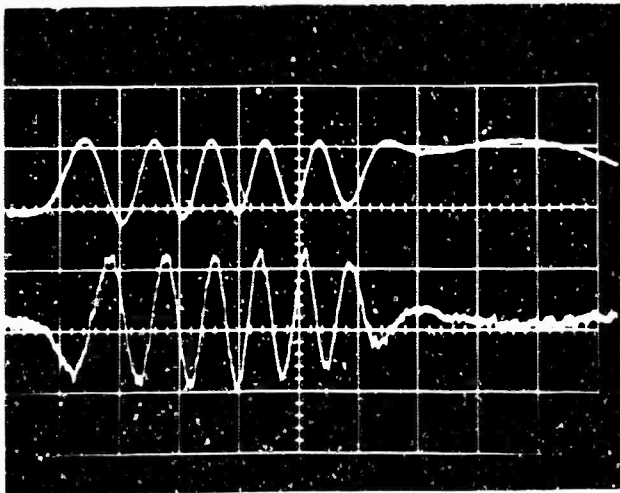


Figure 12. Typical fringe motion as displayed on scope for probe beam along ruby axis. Top signal is ν_{II} , bottom is ν_I . Pump energy is 1.9 kJ. Horizontal scale is 200 microseconds per cm.

• While this does not exclude the existence of strain-induced birefringence, it does suggest that the effect could be rather small. It is planned that in the next period a more detailed study of induced birefringence in ruby will be conducted using polariscopic techniques.

2. Preliminary Gain Studies

As already mentioned, gain measurements were attempted with a passive Q-switch oscillator probe. In the measurement for insertion loss of the ruby (unpumped), it was observed that the ratio of output to input intensity had a spread of 20 to 25 percent. This occurred for the probe beam polarization normal to the principal section, and was independent of the probe amplitude. When the probe beam polarization was in the principal plane, this scatter decreased to about 5 percent (without the ruby in the setup the spread in ratio values was <3 percent). A careful study eliminated the detection apparatus as a source of error, and the difficulty was traced either to the ruby itself or more probably to the passive Q-switch (the output spectrum of the passive Q-switch has not been determined). This investigation is still in progress and will be completed shortly. Some gain measurements were, however, attempted with the passive Q-switch probe with a number of values being averaged. The preliminary results indicate an increase in gain from the center to the edge of the order of 25 percent.

REFERENCES

1. R. L. Townsend, C. M. Stickley, and A. D. Maio, APPL PHYS LETT 7, 94 (1965).
2. A. Y. Cabezas, L. G. Komai, and R. P. Treat, APPL OPT, to be published.

APPENDIX A

DERIVATION OF THE FRINGE RATE EQUATIONS

The optical paths of interest in a Twyman-Green interferometer are shown in Figure A-1. The two paths, x_1 and x_2 , may be written as

$$x_1(t) = x_0(t) - \frac{l(t)}{2}$$

$$x_2(t) = L_2(t) - x_0(t) - \frac{l(t)}{2}$$

where $l(0) \equiv l$, the unpumped rod length. For the case of Interferometer II where the interference fringes are obtained by utilizing the mirrors M_1 and M_2 , the path difference between the two arms, L_1 and L_2 , is given by

$$\Delta_{II} = 2[x_1(t) + nl + x_2(t)] - 2L_1$$

and the phase difference by:

$$\delta_{II} = \frac{2\pi}{\lambda_c} \Delta_{II} = \frac{4\pi}{\lambda_0} [(n-1)l + L_2 - L_1]$$

Here, n is the refraction index at λ_0 , the probe wavelength.

Likewise, for Interferometer I where the fringes arise from reflections off the rod itself,

$$\Delta_I = 2[(x_1 + nl)] - 2x_1$$

or

$$\delta_I = \frac{2\pi}{\lambda_o} [2(x_1 + n\ell) - 2x_1] = \frac{4\pi}{\lambda_o} n\ell$$

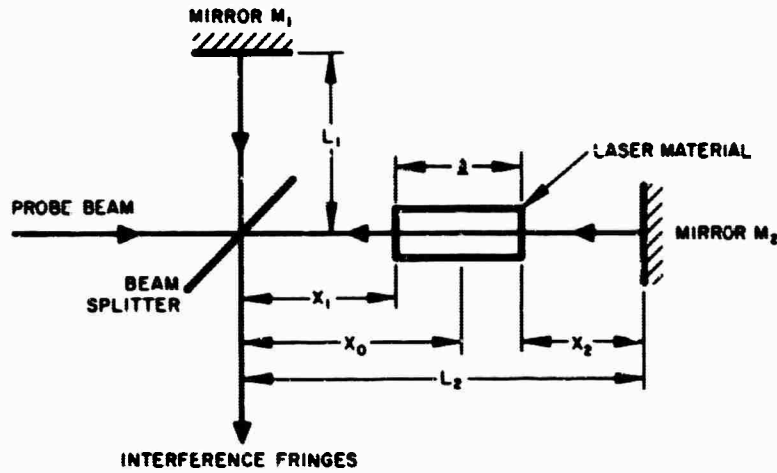


Figure A-1. Definition of interferometer coordinates.

The fringe rates are related to the phase differences δ_I and δ_{II} by

$$\nu_{I, II} = \frac{1}{2\pi} \frac{d}{dt} [\delta_{I, II}]$$

Hence,

$$\begin{aligned} \nu_{II} &= \frac{1}{2\pi} \frac{d}{dt} \left[\frac{4\pi}{\lambda_o} \left[(n - 1)\ell + (L_2 - L_1) \right] \right] \\ &= \frac{2}{\lambda_o} \left[\ell \frac{dn}{dt} + (n - 1) \frac{d\ell}{dt} + \frac{d(L_2 - L_1)}{dt} \right] \end{aligned}$$

But,

$$\frac{dn}{dt} = \frac{\partial n}{\partial T} \frac{\partial T}{\partial t} + \frac{\partial n}{\partial N_o} \frac{\partial N_o}{\partial t}$$

where T is the temperature and N_0 is the ground state population of the laser medium.

Using the definitions,

$$\alpha_\ell \equiv \frac{1}{\ell} \frac{d\ell}{dT} \text{ and } \alpha_n(\lambda) \equiv \frac{1}{n(\lambda)} \frac{dn(\lambda)}{dT}$$

we have that

$$\begin{aligned} \nu_{II} = \frac{2n\ell}{\lambda_0} & \left\{ \left[\frac{(n-1)}{n} \alpha_\ell + \alpha_n \right] \frac{\partial T}{\partial t} + \frac{1}{n} \frac{\partial n}{\partial N_0} \frac{\partial N_0}{\partial t} \right. \\ & \left. + \frac{2}{\lambda_0} \frac{d}{dt} [L_2 - L_1] \right\} \end{aligned}$$

and

$$\nu_I = \frac{2n\ell}{\lambda_0} \left\{ (\alpha_\ell + \alpha_n) \frac{\partial T}{\partial t} + \frac{1}{n} \frac{\partial n}{\partial N_0} \frac{\partial N_0}{\partial t} \right\}$$